Evaluation of Powder and Tableting Properties of Chitosan

Submitted: October 25, 2005; Accepted: June 1, 2006; Published: September 8, 2006

Katharina M. Picker-Freyer[1] and Diana Brink[1]

[1]Martin-Luther-University Halle-Wittenberg, Institute of Pharmaceutical Technology and Biopharmacy, Halle/Saale, Germany

ABSTRACT

The aim of this study was to analyze the process of tablet formation and the properties of the resulting tablets for 3 N-deacetylated chitosans, with a degree of deacetylation of 80%, 85%, or 90%. Material properties, such as water content, particle size and morphology, glass transition temperature, and molecular weight were studied. The process of tablet formation was analyzed by 3-D modeling, Heckel analysis, the pressure time function, and energy calculations in combination with elastic recovery dependent on maximum relative density and time. The crushing force and the morphology of the final tablets were analyzed. Chitosans sorb twice as much water as microcrystalline cellulose (MCC), the particle size is comparable to Avicel PH 200, a special type of MCC, the particles look like shells, and the edges are bent. Molecular weight ranges from 80 000 to 210 000 kDa, the glass transition temperature (Tg) was not dependent on molecular weight. The chitosans deform ductilely as MCC; however, plastic deformation with regard to time and also pressure plasticity are higher than for MCC, especially for Chit 85, which has the lowest crystallinity and molecular weight. At high densification, fast elastic decompression is higher. 3-D modeling allowed the most precise analysis. Elastic recovery after tableting is higher than for MCC tablets and continues for some time after tableting. The crushing force of the resulting tablets is high owing to a reversible exceeding of Tg in the amorphous parts of the material. However, the crushing force is lower compared with MCC, since the crystallinity and the Tg of the chitosans are higher than for MCC. In summation, chitosans show plastic deformation during compression combined with high elasticity after tableting. Highly mechanically stable tablets result.

KEYWORDS: 3-D model, chitosans, compactibility, compression, elastic recovery, morphology.

Corresponding Author: Katharina M. Picker-Freyer, Martin-Luther-University Halle-Wittenberg, Institute of Pharmaceutical Technology and Biopharmacy, Wolfgang-Langenbeck-Str 4, 06120 Halle/Saale, Germany. Tel: +49-345-552 5138; Fax: +49-345-552 7029; E-mail: picker@pharmazie.uni-halle.de

INTRODUCTION

Chitosans are polysaccharides that result after the N-deacetylation of chitin (Figure 1).[1,2] Chemically they are derivatives of cellulose with 2-acetamido-groups instead of 2-hydroxy groups. They consist of β-(1-4)-D-glucosamine. The process of N-deacetylation of chitin can be controlled in its conditions, and according to the conditions different deacetylated chitosans result (40%-98%).[3] Furthermore, the products vary in their degree of polymerization. Chitosan powders have been determined to be crystalline up to 71% deacetylation, further deacetylation leads to a strong decrease in crystallinity and starting from 89% deacetylation crystallinity increases.[4]

Chitin is the second most common polymer and is naturally present in crustacean shells and fungi. The shells of crab, shrimps, and lobster are waste products of the food industry and can be used to produce chitosans.[1,2]

Chitosans are nontoxic, biocompatible, and biodegradable and have been widely used for pharmaceutical purposes,[5-12] and for other purposes such as clarification of waste water, in food products, in feed ingredients, and as a wet strength additive in the paper industry.[1,10] For pharmaceutical use, hydrogels, controlled release dosage forms, mucoadhesive dosage forms, microcapsules, microparticles, and nanoparticles have been developed. For tableting, chitosans have been tested sporadically[13-15]; however, to date no detailed characterization of their compression and compaction behavior exists. Chitosan is also known to reduce friction during tableting[13,16] and to produce controlled release tablets.[17-19] Furthermore, it facilitates soft tableting, which means that it is able to tablet pressure-sensitive materials (eg, enzymes, polymorphic drugs, or enteric-coated pellets without causing extensive damage).[20]

The aim of the present study was to analyze the powder technological, compression, and compaction properties of 3 differently deacetylated chitosans with varying crystallinity in detail and to evaluate the properties of the final tablets. The recently introduced 3-D modeling technique has been used because this method has been successful in characterizing materials with very different deformation mechanisms as well as those with similar deformation mechanisms.

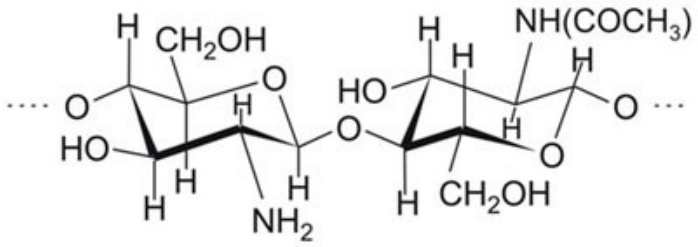

Figure 1. Chemical structure of chitosan.

MATERIALS

The 3 differently deacetylated types of chitosan, Chitosan FG 80 (Chit 80, lot No. TM661), Chitosan FG 85 (Chit 85, lot No. TM611), and Chitosan FG 90 (Chit 90, lot No. TD132) were obtained from Primex Ingredients ASA (Karmsund, Norway). For comparison, microcrystalline cellulose (MCC) (Avicel PH 200, Avi 200, lot No. 11939 C) obtained from FMC Europe NV, Brussels, Belgium, was used.

METHODS

Test Conditions

All materials and tablets were equilibrated, produced, and stored between 35% and 45% relative humidity (RH). Tableting was performed in a special climate-controlled room, which was set to 23°C ± 1°C and 45% ± 2% RH.

Material Properties

Molecular Weight Determination by Field Flow Fractionation

The field flow fractionation (FFF) instrument used for the fractionations was an Eclipse F asymmetrical flow FFF connected to a Dawn EOS multi-angle light scattering detector (Wyatt Technology Europe, Dernbach, Germany) and a RI-101 detector (Shodex, Tokyo, Japan). The intensity of scattered light was measured at 18 different angles. A pump with in-line vacuum degasser (1100 series, Agilent Technologies, Santa Clara, CA) delivered the carrier flow. The ultrafiltration membrane laid on the accumulation wall was made of regenerated cellulose with a cutoff of 10 kDa.

The solvent and carrier for the FFF was acetate buffer with 0.02% NaN_3, which was added to prevent bacterial growth. The sample volume of 100 µL was injected with a flow of 0.2 mL·min^{-1}. Focusing was applied during the injection and was maintained for 1 minute before elution was started. Elution started 6 minutes later. Graded fractionation was applied. For the first 2 minutes the cross-flow was 2 mL·min^{-1}; during the next 5 minutes, it was decreased to 1 mL·min^{-1}, and in the final 17 minutes it was 0 mL·min^{-1}. Analysis was performed between 9 minutes and 25 minutes. Below 9 minutes, the zero signal was visible, above 25 minutes, analysis was not possible because of aggregation of the molecules.[21] Processing of light scattering data was made by the Astra software (Wyatt Technology). The Zimm equation was used with the detectors 5 to 16. In some cases, polynomial fitting was applied. The weight-average molar mass (Mw) and the index of polydispersion (Mw/Mn, where Mn is number of molecules) based on a specific refractive index increment (dn/dc) value given in literature[22] were determined.

Sorption and Desorption Isotherms for Water

Sorption and desorption isotherms were recorded gravimetrically after equilibration at 32% RH. In a preliminary experiment it was demonstrated that equilibrium was reached after 3 days. Thus, the powder was equilibrated at a specific RH over saturated salt solutions[23] for 7 days in triplicate. After equilibration, the powder was weighed and transferred to the next higher RH for equilibration. This procedure started at 32% RH to avoid any drying influence on the sorption characteristics and was performed up to 90% RH. Following that, the samples were moved to the next lower RH downward to 0% RH (phosphorous pentoxide). The water content for each RH was calculated based on the weight of the dry powder as determined at 0% RH.

Water Content

The water content of the materials used in this study was determined by thermogravimetric analysis (TGA) using TGA 209 (Netzsch Gerätebau GmbH, Selb, Germany) in triplicate. The powder was heated with 10 K min^{-1} up to 150°C. Water loss was determined.

Particle Size Determination

Particle size distribution was analyzed by laser light diffractometry using a dry feeder (Sympatec Rodos 12 SR, Sympatec, Remlingen, Germany: pressure, 4 bar; injector beneath pressure, 60 mbar; focal distance, 200 mm; and measuring time, 25-35 seconds) in triplicate. The mean volume particle size distribution was calculated, and the median particle size diameter of this distribution was determined. In addition, for the median diameter, standard deviation was determined from the raw data.

Scanning Electron Microscopy

Both powder and tablets were analyzed by scanning electron microscopy (SEM) (JSM 6400, JEOL, Tokyo, Japan) at an accelerating voltage of 15 kV. Prior to that they were

mounted onto a sample holder and coated with coal/gold/coal (Balzer, Fürstentum, Vaduz, Liechtenstein, type SCD 050).

True Density

The apparent particle density of all of the materials was determined by Helium pycnometry (Accupyc 1330, Micromeritics, Norcross, GA) with 2 repetitions. The equilibrated materials were used for analysis in order to determine the apparent particle density at equilibrium conditions. The method is described by Picker and Mielck.[24]

Bulk and Tap Density

Bulk and tap density were determined in triplicate in a weighed 250-mL cylinder using a volumeter (Erweka GmbH, Heusenstamm, Germany). A quantity of 100 g of the powder was gently filled into the cylinder. Bulk volume was read and bulk density calculated. Following that procedure, the cylinder was tapped at least 2500 times up to a constant volume. Tap volume was read and tap density calculated. Mean and standard deviations were determined.

Carr Index

To analyze flowability, the Carr Index[25] was calculated on the basis of the bulk and tap density. The following equation was used:

$$Carr\ Index = Compressibility[\%] = \frac{Tap\ Density - Bulk\ Density}{Tap\ Density} \times 100 \quad (1)$$

Glass Transition Temperature

The glass transition temperature (Tg) of the dry material was determined using DSC 200 (Netzsch Gerätebau GmbH, Selb, Germany) during the second heating. The sensitivity of the instrument was too low to determine the Tg of the material at equilibrium conditions. Sample size varied between 5 and 10 mg. Heating rate was 40 K min^{-1}. Only with a high heating rate can weak transitions be determined.[26] The temperature interval was set to -50 to 150°C. The Tg was determined by calculating the temperature of the half step height during the second heating. To verify the results, the maximum of the first derivative was also determined.

X-Ray Diffraction Studies

The crystallinities of the powders were compared using a Roentgen diffractometer (URD 63, Freiberger Präzisionsmechanik, Freiberg, Germany). For the radiation, copper with a nickel filter was used. Bragg's angle was analyzed between 3 and 50 2Θ.

Compression Analysis

Tableting

Tableting was performed on an instrumented eccentric tableting machine (EK0/DMS, No. 1.0083.92, Korsch GmbH, Berlin, Germany) with 11-mm-diameter flat-faced punches (Ritter GmbH, Stapelfeld/Hamburg, Germany). Tablets were produced at different graded maximum relative densities ($\rho_{rel,\ max}$): 0.72, 0.76, 0.80, 0.84, and 0.88. The amount of material necessary for each tablet was calculated for each $\rho_{rel,\ max}$ used. The powder mass for each tablet was manually weighed, filled in, and the tablet was produced with an accuracy of ± 0.001 at $\rho_{rel,\ max}$. The tablet height at maximum densification under load was held constant at 3 mm. Displacement of the punch faces was measured by an inductive transducer (W20 TK, Hottinger Baldwin Messtechnik, Darmstadt, Germany). Elastic deformation of the punches and of the machine was corrected.[27] The depth of filling was held constant at 13 mm. The production rate was 10 tablets per minute. No lubricant was used to avoid its having any influence on the microstructure of the tablets.

Ten single tablets were produced at each condition. Data acquisition was performed by a DMC-plus system (Hottinger Baldwin Messtechnik), and data were stored by BEAM-Software (AMS-Flöha, Germany). Force, time, and displacement of the upper punch were recorded for each compaction cycle at a rate of 600 Hz.

Data Analysis

For analyzing tableting data, only data > 1 MPa were used. For 5 compaction cycles of each condition normalized time, pressure, and ln (1/1-D_{rel}) according to Heckel[28] were calculated.

3-D Model

For applying the 3-D modeling technique,[29] all 3 measured values were presented in a 3-D data plot. To this 3-D data plot a twisted plane was fitted by the least-squares method according to Levenberg-Marquard (Matlab, MathWorks Inc, Unterföhrung, Germany) with the following equation. The plane is twisted at $t = t_{max}$.

$$z = \ln\left(\frac{1}{1-D_{rel}}\right) = ((t - t_{max}) \times (d + \omega \times p_{max} - p)) + (e \times p) + (f + d \times t_{max}), \quad (2)$$

where D_{rel} = relative density, t = time, t_{max} = time at maximum pressure, $d = \frac{\delta \ln(1/(1-D_{rel}))}{\delta t}$, ω = twisting angle

at t_{max}, p_{max} = the maximum pressure, p = pressure, $e = \frac{\delta\, ln(1/(1-D_{rel}))}{\delta p}$, and $f = ln\left(\frac{1}{1-D_{rel}}\right)$.

The time plasticity, d, pressure plasticity, e, and fast elastic decompression ,ω, of the 5 compaction cycles at each tableting condition (material and a given $\rho_{rel,\,max}$) were averaged, and means and standard deviations were calculated. The mean standard deviation for d was 0.02; for e, 0.0001; and for ω, 0.0003.

Heckel Function

Heckel describes the decrease of porosity with pressure by first-order kinetics[28]. The Heckel equation is given, which is applicable at the compression part of a porosity pressure plot, is given below.

$$-ln\,\varepsilon \;=\; ln\left(\frac{1}{1-D_{rel}}\right) = \;K\;\times\;p\;+\;A\;, \qquad (3)$$

where ε = porosity, D_{rel} = relative density, K = slope of the Heckel equation, p = pressure, and A = point of intersection with the y-axis.

The slope of the Heckel equation was calculated from the compression part of the plot. A linear fit was produced with an accuracy of R = 0.999 and better. The fit included as much data from the compression part as was possible; an example is given in Figure 2. The determined slope provides information on the total deformation of the powder during the compression phase.

Pressure-Time Function

The pressure-time-function is a repeatedly modified Weibull equation.[30] In the present form[31] it is able to describe the normalized pressure-time curve of the tableting process in an eccentric tableting machine. The equation is as follows:

$$p(t) = P_{O\,max}\left[\frac{t_{end}-t}{\beta}\right]^{\gamma} \tilde{n} e^{1-\left[\frac{t_{end}-t}{\beta}\right]}\gamma, \qquad (4)$$

where p(t) = pressure, $P_{O\,max}$ = maximum pressure of the upper punch, t_{end} = time at the lifting of the upper punch, t = time, β = time difference between the maximum pressure and t_{end}, and γ = parameter of asymmetry of the plot.

The parameter γ is a measure for the resistance of the powder against densification; high values for γ indicate a late and sharp increase of the pressure-time curve. The parameter β indicates the symmetry of the plot; high values indicate high elastic recovery during decompression.

γ and β can be presented in a γ-β-diagram, which provides information on the deformation behavior of the powders. The mean standard deviation for γ was 0.02, and for β it was 0.44.

Force-Displacement Profiles

Force-displacement profiles are used to calculate the different types of energy used for tableting.[32] The analysis includes the compression and decompression of the powder in the die. The area between compression and decompression curve is defined as the compaction energy area. The area between maximum displacement and decompression curve is defined as elastic deformation energy. Both these types of energy were calculated for 5 compaction cycles. Mean and standard deviations were calculated.

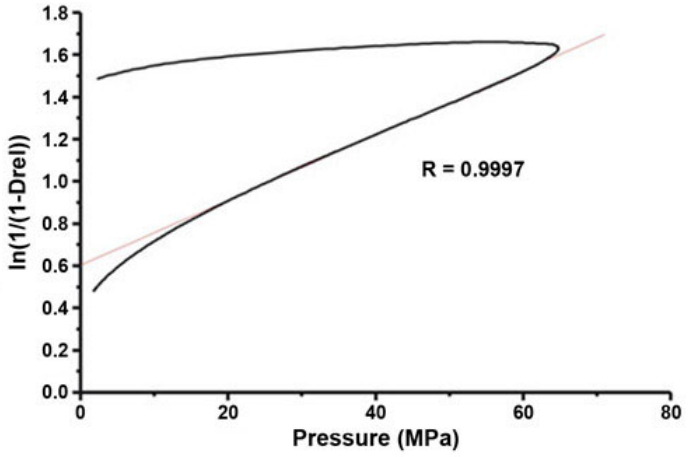

Figure 2. Heckel plot "at pressure" of Chitosan FG 85 at a $\rho_{rel,\,max}$ of 0.80 with an example for determination of the Heckel slope.

Tablet Properties

Elastic Recovery

Elastic recovery after tableting was calculated according to Armstrong and Haines-Nutt[33]:

$$ER(\%) = 100\frac{H_1 - H_{Weg\ maximum}}{H_{Weg\ maximum}}\;, \qquad (5)$$

where ER = elastic recovery, H_1 = height of the tablet after 10 days, and H_0 = minimal height of tablet under load.

The calibrated inductive transducer (W 20 TK, Hottinger Baldwin Messtechnik) was used to measure the axial expansion in the die. The height of the tablet after 10 days was measured by a micrometer screw (Mitutoyo, Tokyo, Japan). Ten tablets were analyzed, and the means and standard deviations were calculated.

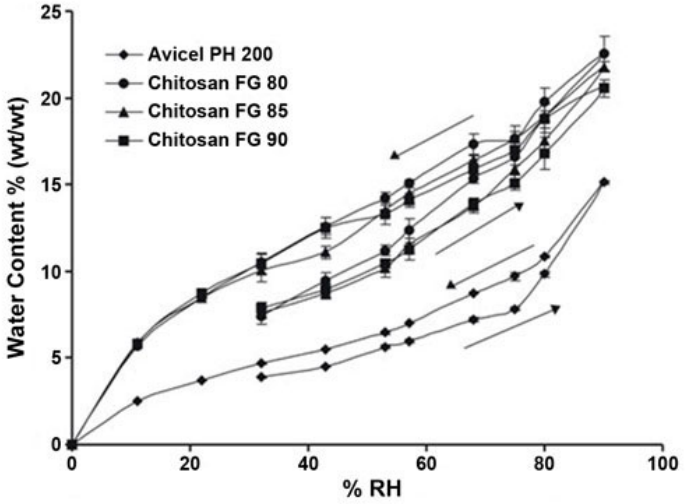

Figure 3. Sorption and desorption isotherms for water of 3 different chitosans compared with MCC (mean ± SD).

In addition, elastic recovery was determined depending on time[34] by thermomechanical analysis at constant temperature over 10 days.

Crushing Force

The crushing force of the tablets was analyzed with the crushing force tester (TBH 30, Erweka GmbH, Heusenstamm, Germany) using a compression rate of 2.3 mm s^{-1} during the crushing force test. For each condition, 5 tablets were analyzed 10 days after tableting, and means and standard deviations were calculated.

Results and Discussion

Material Properties

First, the molecular weight of the 3 chitosans used was determined in duplicate. The median molecular weight of the chitosans is given as follows: for Chit 80, 173.3 ± 5.2 kDa/ 176.6 ± 7.1 kDa; for Chit 85, 87.2 ± 5.2 kDa/ 85.3 ± 5.1 kDa; and for Chit 90, 210.5 ± 6.3 kDa/ 210.7 ± 8.4 kDa. Further, the polydispersion index (Mw/Mn) could be determined to be 2.17 ± 0.09/ 2.21 ± 0.11 for Chit 80, 1.86 ± 0.15/ 1.86 ± 0.13 for Chit 85, and 2.42 ± 0.15/ 2.17 ± 0.11 for Chit 90. The chitosans have a broad molecular weight distribution. Furthermore, the median molecular weights differ between 80 000 and 210 000 kDa. For Chit 85, molecular weight is only half of that of Chit 80 and Chit 90. Molecular weight can influence deformation behavior.

Figure 3 exhibits the water sorption isotherms of the 3 different chitosans when compared with MCC. For all of them the water sorption is higher than it is for MCC. Water sorption goes up to twice that of the sorption for MCC: up to 60% RH ~15% (wt/wt) water was sorbed. In conclusion, the RH during production and storage should be controlled as it was in this study. Further sorption is similar for the 3 chitosans. Table 1 shows the water content of the materials as determined by thermogravimetry. It ranges from 6.83% to 8.47% (wt/wt) and corresponds with the water content measured during sorption. At the RH of the study, the water content increases with increasing deacetylation.

Figure 4 shows the cumulative particle size distribution. Particle sizes are similar to that of Avicel 200, even when the median particle size does not fall in between standard deviation (Table 1); only the particles of Chit 85 are slightly smaller.

The particle shape of the powders is shown in Figure 5. The particles look like shells and the edges are bent. At higher magnification, microstructures become visible and little particles are spread on the surface of the powders. The particle structure is more or less the same for the 3 different types of chitosan.

In Table 1, the apparent particle, tap, and bulk densities of the materials are given. Apparent particle density increases slightly with higher N-deacetylation; Chit 90 exhibits the highest apparent particle density. Bulk and tap density are dependent on particle size. For Chit 85, bulk and tap density are higher than for Chit 80 and Chit 90, which can be seen in congruence with the lower particle size.

Table 1. Powder Technological Properties of 3 Different Types of Chitosan*

Material	Quality	N-Deacetylation (%)	Water Content % (wt/wt)	Median Particle Size (μm)	True Density (g/cm³)	Bulk Density (g/cm³)	Tap Density (g/cm³)	Carr Index (%)
Chitosan	Chitosan food grade 80	80	6.83 ± 0.03	160 ± 1	1.468 ± 0.002	0.280 ± 0.000	0.373 ± 0.006	24.70 ± 1.15
Chitosan	Chitosan food grade 85	85	8.18 ± 0.03	120 ± 1	1.473 ± 0.001	0.366 ± 0.006	0.500 ± 0.000	26.87 ± 1.27
Chitosan	Chitosan food grade 90	90	8.47 ± 0.07	170 ± 1	1.497 ± 0.002	0.228 ± 0.001	0.334 ± 0.027	31.86 ± 0.03
MCC	Avicel PH 200	-	4.03 ± 0.12	180 ± 1	1.5750.001	0.4290.021	0.5020.002	14.614.11

*All values are expressed as mean ± SD.

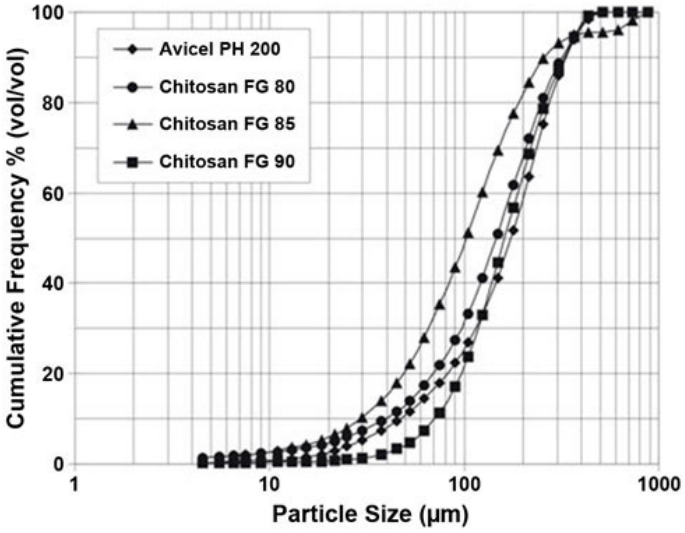

Figure 4. Particle size determined by laser diffraction of 3 different chitosans and MCC (mean ± SD).

Bulk and tap density can provide information on the flowability of the powders, and hence while using both these values, the Carr Index was calculated. The lower the Carr Index is, the better the flowability of the powder.[25] According to Carr, values of 5 to 10, 12 to 16, 18 to 21, and 23 to 28 represent excellent, good, fair, and poor flow properties, respectively. Thus, all chitosans show poor flowability. However, flowability increased with increasing N-deacetylation; Chit 80 showed the lowest Carr Index and thus the highest flowability with a value of 24.70 (Table 1).

The material deformation is dependent on its Tg. For the different types of chitosan, the following values for Tg were determined for the dry material: 102.6°C ± 6.4°C (Chit 80), 107.9°C ± 5.8°C (Chit 85), 88.8°C ± 5.1°C (Chit 90). Any influence on molecular weight could not be detectable. Since the powders contain only small amounts of amorphous material, the sensitivity of the DSC apparatus used was too low to determine the Tg at equilibrium conditions. However, with increasing humidity, it can be assumed that the Tg decreases.[26] For completely amorphous chitosan a Tg of 82.2°C is given in literature.[35]

Tableting

The tableting behavior was characterized by 3-D modeling (Figure 6). Heckel analysis (Figure 7A), parameter determination of the pressure-time function (Figure 7B),

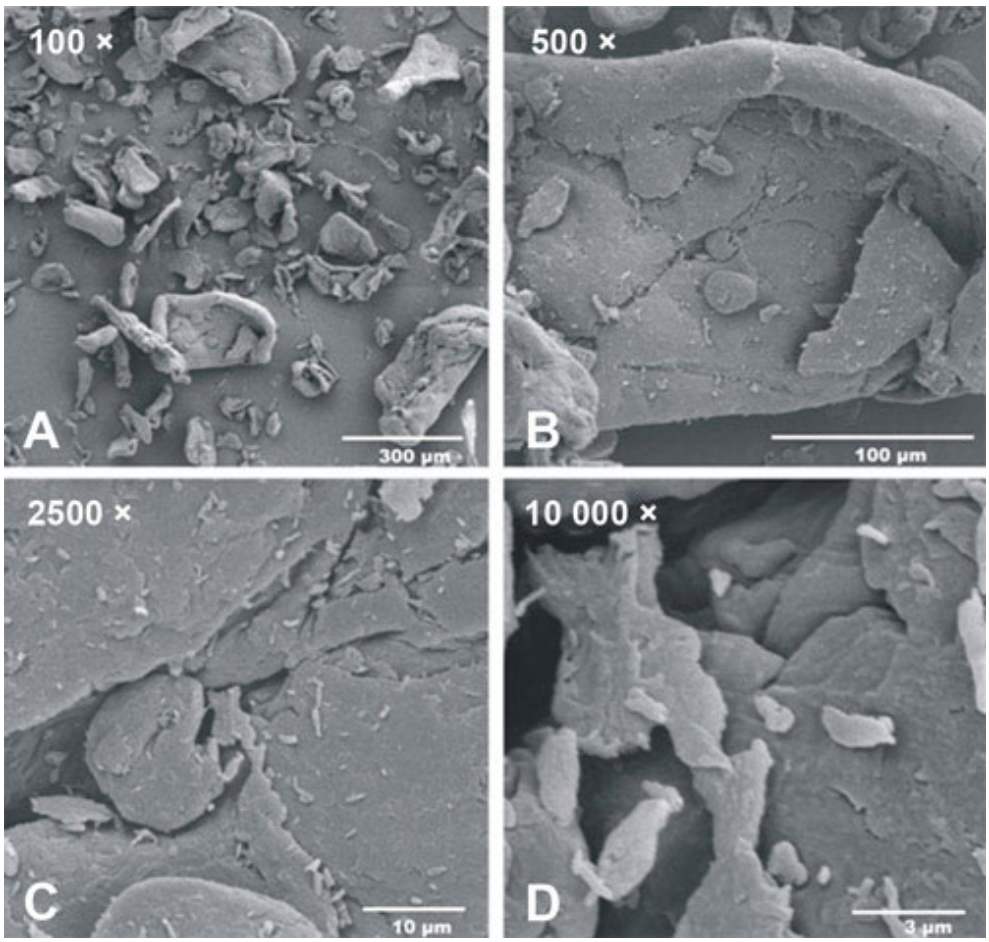

Figure 5. SEM of Chitosan FG 85 powder exemplarily.

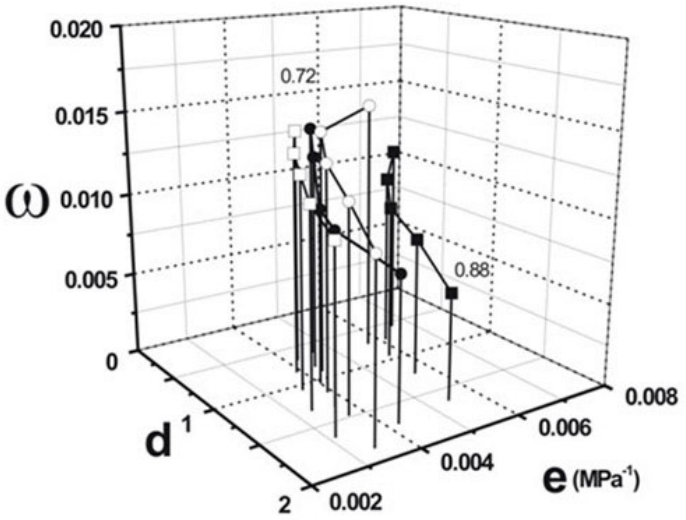

Figure 6. 3-D parameter plot in dependence on $\rho_{rel,\ max}$ (0.72-0.88) of Avicel PH 200 (□), Chitosan FG 80 (■), Chitosan FG 85 (○), and Chitosan FG 90 (●).

and energy calculations from the force-displacement profile (Figures 7C and D) were used in comparisons.

Figure 6 shows the 3 different types of chitosan in comparison to MCC when analyzed by 3-D modeling. They all show a higher pressure plasticity e than MCC and the time plasticity d is also higher. Fast elastic decompression indicated by ω was found to be similar to MCC, with the exception of Chit 85. The higher Chit 85 ω might be caused by its lower molecular weight. The deformation behavior of the chitosans changed continuously with increasing $\rho_{rel,\ max}$. Furthermore, crystallinity and the crystallinity index (CI) decrease in the following order: CI(Chit 80) > CI(Chit 90) > CI (Chit85).[4] Since crystallinity can influence deformation, it is clear why an increase in pressure plasticity e and a decrease in time plasticity d follow this order. Determinations done by X-ray diffractometry showed no differences in crystallinity, when considering an error of determination of 5% to 10%.[36] However, according to van Luyen and Mai Huong,[4] the differences in crystallinity are slight. Another possible explanation for the different deformation behavior could be different particle size distribution as described above in Material Properties.

Figure 7A shows the slope of the Heckel function for the different chitosans. In this case, Chit 85 behaves in a similar way to MCC, and both the other types Chit 80 and Chit 90 show a lower Heckel slope and thus higher resistance against deformation. It must be noted that according to the degree of N-deacetylation no order could be set up. The higher Heckel slope and thus a higher and easier deformation of Chit 85 in comparison to both the other chitosans might depend on the lower molecular weight of Chit 85. However, the determination of the Heckel slope includes plastic and elastic deformation and is therefore less precise than the pressure plasticity e of the 3-D model.

Figure 7B shows the results of the analysis with the pressure time function in the γ-β-diagram. Both Chit 80 and

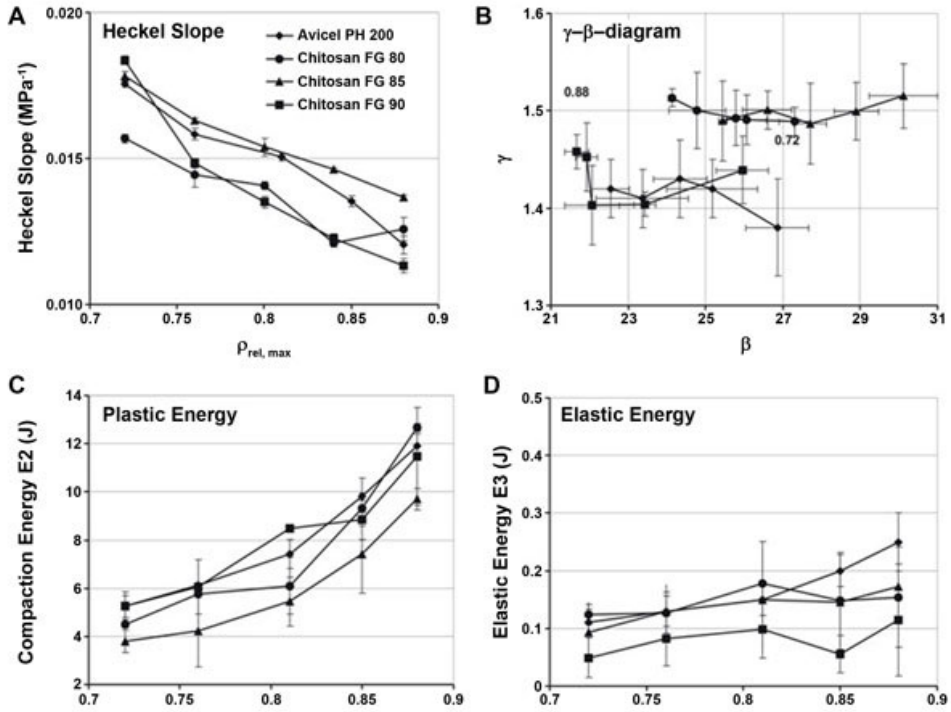

Figure 7. Heckel slope, β-γ-diagram, plastic and elastic energy in dependence on $\rho_{rel,\ max}$ determined for 3 different chitosans and MCC (in graph B, $\rho_{rel,\ max}$ decreases for each curve from left (0.88) to right (0.72); mean ± SD).

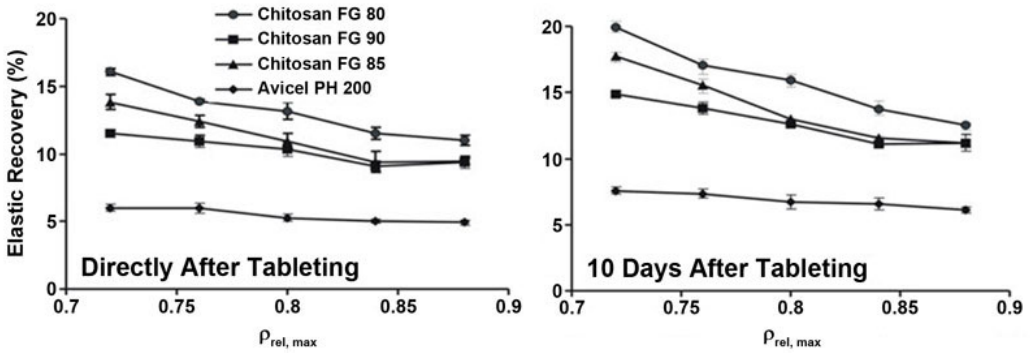

Figure 8. Elastic recovery in dependence on $\rho_{rel, max}$ of 3 different chitosans and MCC (mean ± SD).

Chit 90 are more elastic than MCC, which is indicated by the much higher β- and γ-values. Moreover, Chit 85 behaves similarly to MCC as in case of the Heckel function. In conclusion, it can be stated that the deformation behavior is the opposite of what was derived from the Heckel slope. However, the factor time is the main focus of this analysis and the time-dependent deformation is shown. The result is in agreement with time plasticity d from 3-D modeling, which was similar for Chit 85 and MCC.

Finally, Figures 7C and D exhibit compaction and elastic energy, which was determined by force-displacement profiles. Compaction energy of the chitosans is similar to that of MCC except for Chit 85: this might be caused by the lower particle size of Chit 85. Elastic energy is in between the standard deviation for MCC, Chit 80, and Chit 85; and for Chit 90, it is slightly lower. In between the chitosans, the following order for elastic energy (EE) can be set up: EE(Chit 90) < EE(Chit 85) ≤ EE(Chit 80).

In summation, plastic deformation with regard to time and also pressure plasticity are higher than for MCC, especially for Chit 85, which has the lowest crystallinity and molecular weight. At high densification, fast elastic decompression is higher.

When comparing the different analysis techniques, it becomes evident that 3-D modeling allows for the most precise analysis. The results determined with the Heckel analysis mainly present pressure plasticity e; the results determined with the pressure-time function mainly present time plasticity d, and energies derived from force-displacement profiles mainly provided information that was similar to pressure plasticity (compaction energy) and fast elastic decompression (EE). In summation, the results show that the

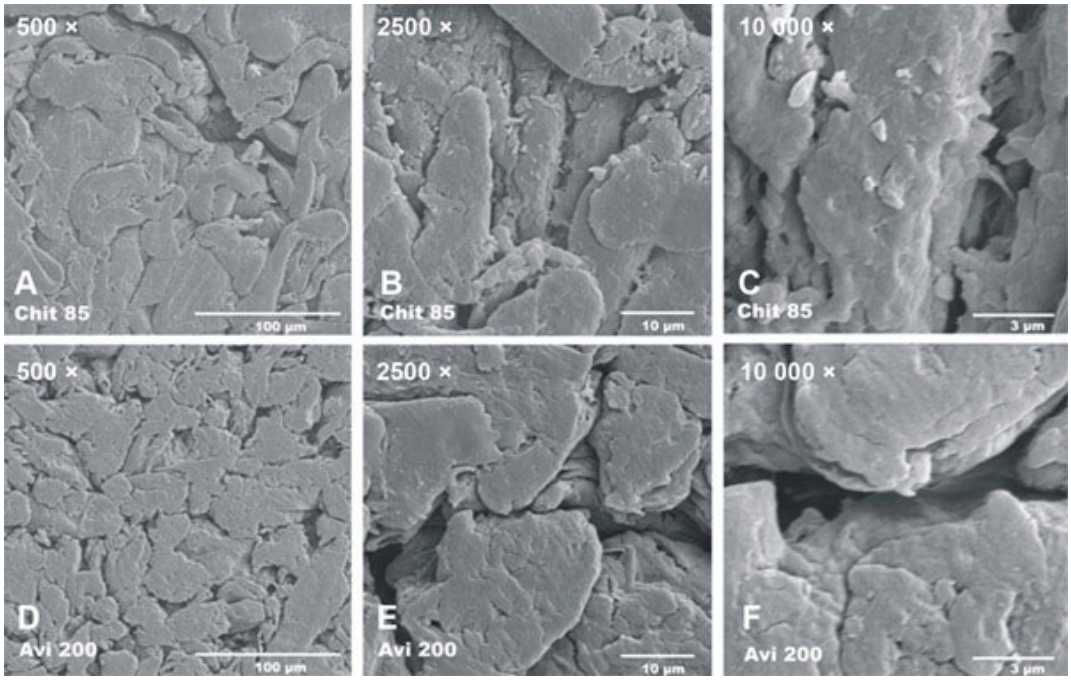

Figure 9. SEM of the surface of tablets of Chitosan FG 85 and MCC.

3-D modeling technique completely characterizes deformation, and it is able to differentiate in 1 step between time-dependent and pressure-dependent deformation.

Final Formation of the Tablets

Figure 8 shows the elastic recovery of the different chitosan tablets when compared with MCC tablets: relaxation that had already started during tableting continues. Elastic recovery for the chitosan tablets is higher than that of the MCC tablets. This fact is in contradiction to the determined EE, which was lower for the chitosans. Obviously fewer bonds are formed inside the chitosan tablets when compared with MCC tablets. Elastic recovery is slightly different for the 3 different types of chitosan (eg, it increases with decreasing N-acetylation). For tablets made of Chit 80, elastic recovery is the highest, and for tablets made of Chit 90 it is the lowest. Summing up, the process of tablet formation to an equilibrium state considerably continues after tableting. Thus, to describe the process of tablet formation completely elastic recovery after tableting was determined depending on time (data not shown). Twenty-four hours after tableting, expansion was measured, and the following 9 days no further elastic recovery occurred. Thus elastic recovery was complete.

Tablet Properties

As shown in Figure 9, chitosan tablets were analyzed on the upper surface by SEM after relaxation. Similar to MCC (Avi 200) the surface appears smooth and the particles are strongly deformed and appear to be glued together. At higher magnification, a network-like structure results. It has been shown that drugs with a melting point between 50°C and 95°C can partially melt during tableting.[37] These temperatures can be locally achieved during tableting. Therefore, it can be assumed with regard to MCC, chitosan Tg can be reversibly exceeded during tableting[26]; hence following tableting, the tablet cools down and a stable tablet results. For MCC, the Tg at equilibrium conditions is 60°C to 80°C, for chitosans the Tg is 90°C to 110°C for the dry material, and it will be lower at higher levels of humidity.

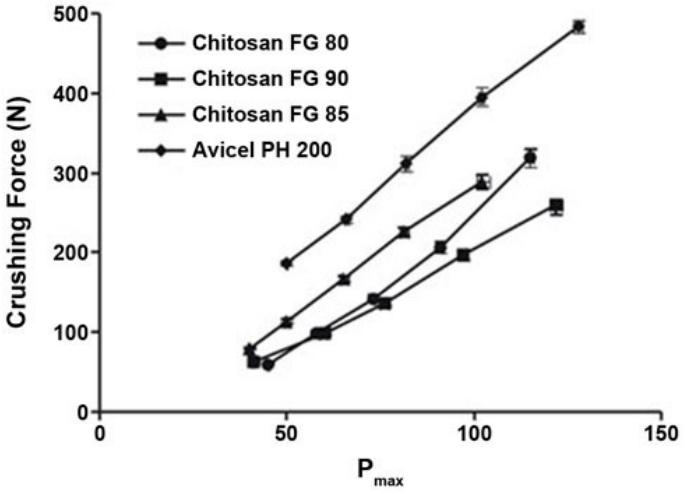

Figure 10. Compactibility plot of 3 different chitosans and MCC (mean ± SD).

This assumption as derived from SEM can be underlined by the results on the crushing force and the compactibility of the chitosans. The compactibility is high; crushing force was measured to be almost 300 N (Figure 10) at moderate maximum upper punch pressure of ~100 MPa. This crushing force is lower than for MCC; however; crystallinity is higher than in case of MCC and the reversible exceeding of Tg occurs only in the amorphous material, which might lead to lower crushing forces when compared with MCC. Thus, it can be concluded that chitosan is well qualified for tableting.

CONCLUSIONS

The chitosans show tableting and tablet properties that are similar to those of MCCs. Deformation behavior could be best described by using 3-D modeling. The crushing force is high, and a network-like structure is visible with SEM, moreover this structure can be attributed to a reversible exceeding of Tg during tableting as is the case for MCC. It must also be mentioned that the most distinct difference found when compared with MCC is that elastic recovery is high and thus more mechanical energy is released after tableting. This behavior allows for the application of chitosans to be used for "soft tableting" of pressure-sensitive materials.[20]

ACKNOWLEDGMENTS

The authors gratefully acknowledge Dr. -Ing. K. Legenhausen, Institute of Mechanical Engineering, Technical University Clausthal-Zellerfeld, for the use of laser light diffractometry; Christian Augsten for his work with molecular weight determination by FFF; and Primex Ingredients of Karmsund, Norway, for donating the chitosans.

REFERENCES

1. Hudson SM, Smith C. Polysaccharides: chitin and chitosan: chemistry and technology of their use as structural materials. In: Kaplan DL, ed. *Biopolymers From Renewable Sources.* Berlin, Germany: Springer; 1998:96–118.

2. Hirano S. Chitin and chitosan. *Ullmann's Encyclopedia of Industrial Chemistry [book on CD-ROM].* New York, NY: John Wiley & Sons Inc; 2000.

3. Pavlath AE, Wong DWS, Robertson GH. Chitosan (preparation, structure, and properties). In: Salamone JC, ed. *Polymeric Materials*

Encyclopedia [Book on CD-ROM]. Boca Raton, FL: CRC Press Inc; 1996.

4. van Luyen D, Mai Huong D. Chitin and derivatives. In: Salomone JC, ed. *Polymeric Materials Encyclopedia [Book on CD-ROM].* Boca Raton, FL: CRC Press Inc; 1996.

5. Felt O, Buri P, Gurny R. Chitosan: a unique polysaccharide for drug delivery. *Drug Dev Ind Pharm.* 1998;24:979–993.

6. Genta I, Perugini P, Pavanetto F. Different molecular weight chitosan microspheres: influence on drug loading and drug release. *Drug Dev Ind Pharm.* 1998;24:779–784.

7. Illum L. Chitosan and its use as a pharmaceutical excipient. *Pharm Res.* 1998;15:1326–1331.

8. He P, Davis SS, Illum L. Sustained release chitosan microspheres prepared by novel spray drying methods. *J Microencapsul.* 1999; 16:343–355.

9. Lueßen HL, Rentel CO, Kotzé AF, et al. Mucoadhesive polymers in peroral peptide drug delivery. IV. Polycarbophil and chitosan are potent enhancers of peptide transport across intestinal mucosae in vitro. *J Control Release.* 1997;45:15–23.

10. Paul W, Sharma CP. Chitosan, a drug carrier for the 21st century: a review. *STP Pharma Sci.* 2000;10:5–22.

11. Remunan-López C, Portero A, Vila-Jato JL, Alonso MJ. Design and evaluation of chitosan/ethylcellulose mucoadhesive bilayered devices for buccal drug delivery. *J Control Release.* 1998;55:143–152.

12. Yamamoto H, Takeuchi H, Hino TK, Kawashima Y. Mucoadhesive liposomes: physicochemical properties and release behavior of water-soluble drugs from chitosan-coated liposomes. *STP Pharma Sci.* 2000;10:63–68.

13. Sawayanagi Y, Nambu N, Nagai T. Directly compressed tablets containing chitin or chitosan in addition to lactose or potato starch. *Chem Pharm Bull (Tokyo).* 1982;30:2935–2940.

14. Sawayanagi Y, Nambu N, Nagai T. Directly compressed tablets containing chitin or chitosan in addition to mannitol. *Chem Pharm Bull (Tokyo).* 1982;30:4216–4218.

15. Knapczyk J. Excipient ability of chitosan for direct tableting. *Int J Pharm.* 1993;89:1–7.

16. Yao T, Yamada M, Yamahara H, Yoshida M. Tableting of coated particles. II. Influence of particle size of pharmaceutical additives on the protection of coating membrane from mechanical damage during compression process. *Chem Pharm Bull (Tokyo).* 1998;46:1510–1514.

17. Sawayanagi Y, Nambu N, Nagai T. Use of chitosan for sustained-release preparations of water-soluble drugs. *Chem Pharm Bull (Tokyo).* 1982;30:4213–4215.

18. Henriksen I, Skaugrud O, Karlsen J. Use of chitosan and chitosan malate as an excipient in wet granulation of three water soluble drugs. *Int J Pharm.* 1993;98:181–188.

19. Rege PR, Shukla DJ, Block LH. Chitinosans as tableting excipients for modified release delivery systems. *Int J Pharm.* 1999;181:49–60.

20. Picker KM. Soft tableting: a new concept to tablet pressure sensitive drugs. *Pharm Dev Technol.* 2004;9:107–121.

21. Anthonsen MW, Vårum KM, Hermansson AM, Smidsrød O, Brant DA. Aggregates in acidic solutions of chitosans detected by static laser light scattering. *Carbohydr Polym.* 1994;25:13–23.

22. Beri RG, Walker J, Reese ET, Rollings JE. Characterization of chitosans via coupled size-exclusion chromatography and multi-angle laser light-scattering technique. *Carbohydr Res.* 1993;238:11–26.

23. Greenspan L. Humidity fixed points of binary saturated aqueous solutions. *J Res Natl Bureau Stand-A Phys Chem.* 1977;81:89–96.

24. Picker KM, Mielck JB. True density of swellable substances at different relative humidities: a new approach to its determination. *Eur J Pharm Biopharm.* 1996;42:82–84.

25. Carr RL. Evaluating flow properties of solids. *Chem Eng.* 1965;72:163–168.

26. Picker KM. The relevance of glass transition temperature for the process of tablet formation. *J Therm Anal Calorim.* 2003;73: 597–605.

27. Picker KM. New Insights Into the Process of Tablet Formation – Ways to Explore Soft Tableting. *Habilitationsschrift Universität Halle-Wittenberg.* Marburg, Germany: Görich und Weiershäuser Verlag; 2002.

28. Heckel RW. An analysis of powder compaction phenomena. *Trans Metallurg Soc AIME.* 1961;221:1001–1008.

29. Picker KM. A new theoretical model to characterize the densification behavior of tableting materials. *Eur J Pharm Biopharm.* 2000;49: 267–273.

30. Dietrich R, Mielck JB. Parametrisierung des zeitlichen Verlaufs der Verdichtung bei der Tablettierung mit Hilfe der modifizierten Weibull-Funktion. *Pharm Ind.* 1985;47:216–220.

31. Konkel P, Mielck JB. Associations of parameters characterizing the time course of the tableting process on a reciprocating and on a rotary tableting machine for high-speed production. *Eur J Pharm Biopharm.* 1998;45:137–148.

32. Dürr M, Hanssen D, Harwalik H. Kennzahlen zur Beurteilung der Verpreßbarkeit von Pulvern und Granulaten. *Pharm Ind.* 1972;34: 905–911.

33. Armstrong NA, Haines-Nutt RF. Elastic recovery and surface area changes in compacted powder systems. *J Pharm Pharmacol.* 1972; 24:135P–136P.

34. Picker KM. Time dependence of elastic recovery for characterization of tableting materials. *Pharm Dev Technol.* 2001;6:61–70.

35. Mo X, Tu T, Zhou H. Crystallization kinetics of chitosan. *Gonneng Gaofenzzi Xuebao.* 1996;9:102–112.

36. Saleki-Gerhardt A, Ahlneck C, Zografi G. Assessment of disorder in crystalline solids. *Int J Pharm.* 1994;101:237–247.

37. Schmidt J. *Direkttablettierung niedrigschmelzender nichtsteroidaler Antirheumatika mit mikrokristallinen Cellulosen [dissertation].* Halle/Saale, GermanyUniversität Halle-Wittenberg; 1997.